Waveform Measurement Unit-based Fault Location in Distribution Feeders via Short-Time Matrix Pencil Method and Graph Neural Network

Mohammad MansourLakouraj, *Student, IEEE,* Hadis Hosseinpour, *Student, IEEE,* Hanif Livani, *Senior Member, IEEE* and Mohammed Benidris, *Senior Member, IEEE*

***Abstract*—This paper proposes the use of the Short-Time Matrix Pencil method (STMPM) technique and Graph Neural Network (GNN) for fault location in active distribution feeders based on an emerging class of sensors, known as Waveform Measurement Units (WMUs). WMUs record synchronized voltage and current waveforms in the time domain with high sampling rates. The proposed fault location framework consists of two stages. In the first stage, STMPM is adopted to capture the dominant modes of the transient changes of WMUs' sinusoidal signals due to faults in different locations of the distribution grid. The second stage is to use a grid-informed GNN model to identify the fault location and type using the captured features of the signal before, during, and post-fault with STMPM. GNN can capture the spatial-temporal relationship between data from different sensors in different locations to enhance situational awareness and fault location accuracy. The proposed method is examined on a modified IEEE network with distributed energy resource (DER) and for transient symmetrical and asymmetrical faults under different loading, DER generation level, noises, and sensors' sampling rate conditions. The results show the merits of the proposed two-stage fault location framework compared to the conventional approaches; while a challenging problem is addressed in active distribution grids.**

***Index Terms*—Active distribution networks, Fault location, Short-Time Matrix Pencil Method, Graph Neural Network, Waveform Measurement Units.**

I. Introduction

POWER distribution grids can experience various types of faults that cause outages of power supply, endangering safety, and apparatus failures [1]. It is crucial to locate these faults and identify their types for finding the vulnerable points of the grids for future maintenance or performing restoration quickly by clearing the cause of faults in the detected location. Therefore, an efficient fault locator would enhance reliability and situational awareness in power distribution grids. On the other hand, the proliferation of distributed energy resources (DERs) at the distribution level increases the need for equipping grids with more advanced measurement devices such as phasor measurement units (PMUs) and waveform measurement units (WMUs) for better monitoring and control [2], [3]. Thus, the recorded data by these emerging sensors provide an opportunity to develop more accurate fault location and event analysis tools.

This work was supported by the U.S. National Science Foundation (NSF) under Grant ECCS-2033927. *Corresponding author*: Mohammad MansourLakouraj. The authors are with the Department of Electrical and Biomedical Engineering, University of Nevada, Reno, Reno, NV 89557 USA (e-mail: mansour@nevada.unr.edu; hhosseinpour@unr.edu; hlivani@unr.edu; mbenidris@unr.edu).

A. Motivation and Challenges

Transient faults, known as short-duration faults, happen in distribution grids frequently due to several reasons, such as incipient faults. An incipient fault happens because of damaging insulation of grid components, animal and tree contacts, and weather conditions [4]. Incipient faults have self-clearing capability within a short period of time, varying from sub-cycle (a quarter of a cycle) to multi-cycles (four cycles) [5]. Since the duration of these faults is very small, it is very challenging to identify the location of these faults and perform proper maintenance actions to prevent the future permanent and catastrophic faults. Localization of such challenging incipient faults and similar transient faults have motivated us to use synchronized waveform measurements provided by an emerging class of sensors named WMUs [6]. A high sampling rate of WMUs, which can go up to 256 samples-per-cycle and even higher [7], enables the grid operators to monitor sudden changes in voltages and currents [2]. In sharp contrast, phasor measurement units (PMUs), which were previously used at transmission-level [8], [9], and now are becoming popular in distribution grids for increasing situational awareness [10], have much slower sampling rate to capture transient events in a very short period of time. The sampling rate of PMUs are ranging from 30 to 120 samples-per-second [11], meaning that PMUs can record at most 2 samples per cycle which are remarkably less than 256 recorded samples of WMUs in each cycle. Therefore, sudden changes of signals due to transient faults or events, recorded by PMUs, may not contain all the required information for proper event analysis in a short period of time and may be seen as a normal event or variation [12]. Additionally, it is worth mentioning that other faults with a longer duration of time or permanent faults without self-clearing features are required to be studied and located, as they can cause catastrophic consequences for the grids and endanger safety if they are not cleared within a short time by protection devices. Therefore both transient and permanent/longer duration faults are located and identified in this study.

Furthermore, realizing the spatial correlation of sensors can be beneficial in improving fault location accuracy [13]. This correlation can be captured by physics-informed graph-based approaches containing the physical distance metrics of WMUs as well as temporal information of signals such as voltage or current measurements in each node or location. Due to the

high sampling rate of WMUs, the length of the raw data will be large and contain unnecessary and redundant information, which increases the computation time significantly and requires expensive resources for handling such large data sets. Moreover, the long duration of the data stream, especially before and after faults may not contain useful information to improve the performance of fault location. Even during a fault, the sudden changes may be interpreted as noise on raw data, and therefore a robust feature-extracting approach is crucial to characterize the transient events and recognize the meaningful oscillations due to faults. Furthermore, these WMU sensors are expensive devices, and distribution grids may only be equipped with a few of them. The scarcity of WMU data is then another challenge considered in this paper.

B. Related studies

Research studies on the classification and localization of faults in distribution networks are classified into three groups such as model-based, data-driven-based, and hybrid physics-aware data-driven approaches. Authors in [14] propose an impedance-based approach in which the fundamental phasor elements of signals are implemented for narrowing down the potential faulty nodes list. Then, the authors use search-based techniques to find the fault location(s) using the voltage changes on various monitored buses of distribution systems. The proposed study in [15] applies traveling wave-based techniques, using the reflected monitored waves from different locations for identifying faulty regions. This technique needs ultra-high sampling rate sensors for measurement, which are emerging in distribution systems. The fault classification and localization problems are addressed in [16] using a limited number of PMU data and a convolution neural network algorithm to enhance the resiliency of the grid.

Different model-based and data-based approaches have been proposed for locating and classifying *transient* and *incipient* faults in distribution networks. Reference [2] implements Prony modal analysis to extract the modes of raw signals captured by WMUs. The obtained modes are then used for building circuits to locate transient faults and events. However, methods focusing on circuit-based analysis and modeling can be a challenging option considering the complexity of the three-phase unbalance networks equipped with different devices, mutual impedance, and randomness of the events. As for data-driven model studies, human-level concept learning is adopted in [17] to decompose waveform signals into residuals and segments of the shape. Then, the probabilistic learning-based technique is used to classify the incipient faults. This problem does not focus on the event location, and the physics of the grid is neglected in the identification process. In a recent study, a short-time Fourier transform (STFT) and dual-channel CNN classifier are proposed to identify the cause of different faults with waveform data [18]. In [19], an early fault identification technique is presented using the Siamese temporal graph network in passive distribution grids. This technique converts the waveform data into a temporal graph network model for classifying the fault types and other transient events such as load and capacitor switching. The problem does not focus on the localization of the events in active grids, and the network topology is not included in the proposed algorithm. In most of the data-based models, the physical characteristics of the grid are ignored, unlike the model-based problems. Recently, a network-aware data-driven model called graph neural network (GNN) has been proposed [20] which can link the gaps between data-based and model-based studies for fault location and classification problems. In [21] and paper [13], GNN is used for localizing fault in passive and active distribution systems using phasor measurement data, respectively. GNN is also applied for PMU-based event classification [22], [23] and clustering [24] in distribution systems. However, the current studies have not investigated the emerging WMU sensors and precise feature extraction techniques for handling the high-resolution waveform data besides the application of graph-based learning methods in power distribution feeders.

C. Contributions

This paper proposes an efficient feature extraction technique, named the short-time matrix pencil method (STMPM), and a network-aware GNN model for identifying the fault location and type in active distribution networks using the recorded synchro waveform data. The contributions of the proposed study are listed as follows:

- This paper mainly addresses the challenging transient fault location problem. This is challenging as transient faults occur in a short period of time, e.g., one cycle, and usually have the self-clearing ability, making them hard to detect. Permanent faults are also located using the proposed study, which are instantly more life-threatening and hazardous for grid equipment.
- The Syncro waveform voltage information is captured by a high-sampling rate emerging class of sensors in active distribution grids, before and after the occurrence of faults. The feature extraction technique, STMPM, decomposes the high sampling rates of WMUs in a sliding window into dominant modes consisting of damping factors and angular frequencies. Unlike the matrix pencil method (MPM), STMPM captures oscillations over the sliding time window at each snapshot of the data stream and records the dominant modes in each snapshot [25].
- Graph neural network (GNN) is implemented in the fault location stage by capturing the spatial correlation of WMU data in the limited number of nodes across the distribution feeders. The proposed GNN incorporates the physical characteristic of the power network as a weighted graph with nodes containing the sensor data. This method links the pure data-driven method with grid-aware analysis for enhancing the fault location and classification accuracy.

Therefore, unlike our previous study presented as a poster in the Electrical safety workshop (ESW), which focused on fault location problems with GNN and PMU data, this paper addresses the same graph-based fault location problem with a focus on synchro waveform data and STMPM feature engineering approach. The rest of the paper is organized as follows. Section II explains the feature engineering method. Section III discusses the grid-informed model. Case studies

and simulation setup are explained in Section IV. Section V and VI present the numerical experiments and discussion, respectively. Section VII concludes the study.

II. Feature Engineering of Measured signals

The space vectors of a three-phase voltage signal are in (1) where the real and imaginary terms correspond to α and β elements of the Clark transform. To simplify a three-phase set of voltage signals and analyze their instantaneous behavior, the space vectors are well-suited. Under the occurrence of events, $Y(t)$ and $Z(t)$ show distorted ellipse in the complex plane, that can be used for models using image-based fault or event classification with CNN [12], [26]. However, each of these terms ($Y(t)$ and $Z(t)$) also contains information on the original three phases observed by WMU sensors. Thus, the real part of space vectors is used as a time-based signal in our analysis [27] not only to shrink the data dimension for reducing computational time but to capture the distortion in all three-phase voltage signals together all in an informative signal Y.

$$\begin{aligned} y(t) &= \frac{2}{3}\left[\, y_a(t) + \; e^{j\,\frac{2\pi}{3}}\, y_b(t) \; + \; e^{j\,\frac{-2\pi}{3}}\, y_c(t)\,\right] \\ &= Y(t) \; + j\, Z(t) \end{aligned} \tag{1}$$

A. Theoretical Background of Signal Reconstruction

The signal in a period T is defined by a summation of sinusoidal terms in the Fourier series as given in (2). In (2), $Y(t)$ is expanded by sinusoidal terms with residues $\Psi_i \angle \theta_i$ considering the period of T. Also, N represents the number of terms that need to be considered for reconstructing the signal $Y(t)$, and i is the term number.

$$Y(t) = \sum_{i=1}^{N} \Psi_i \;\cos\left(2\pi i\,\frac{t}{T} + \theta_i\right) \tag{2}$$

Equation (2) can be represented in a different way as (3), considering $f = \frac{1}{T}$, $\omega_i = 2i\pi f$ and the summation of damped sinusoidal terms.

$$Y(t) = \sum_{i=1}^{N} \Psi_i \; e^{-\alpha_i\, t} \;\cos\left(\omega_i\, t + \theta_i\right) \tag{3}$$

In (3), α_i is damping factor in sec^{-1} and ω_i is angular speed in $rad.sec^{-1}$, which are real and imaginary parts of the complex frequency $\alpha_i \pm j\omega_i$, respectively. If $\alpha_i = 0$, equations (2) and (3) are equal $\forall i$. Different methods are used for determining complex frequencies and residues in equation (3), including Prony [28] and matrix pencil method (MPM) [29], but MPM demonstrates better results [29], [30].

It is common that a signal restricted within a sliding window to be defined with a few terms. A portion of the voltage signal is shown in Fig. 1 in a window with the length of T_w. T_w is equal to one power cycle and the recorded signal by WMUs consists of 5 cycles. The window moves along the sample axis and in each snapshot, the MPM is applied to capture all signal features within the window. This method is called STMPM, deriving the time-indexed complex frequencies [31].

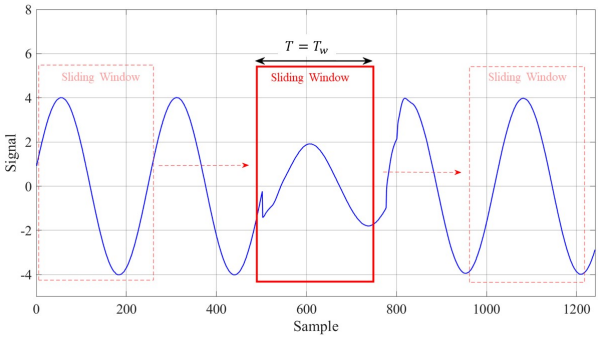

Fig. 1. Sinusoidal signal and sliding window

B. STMPM Formulation

The mathematical representation of STMPM is discussed in this sub-section [32]. The matrix X is formed using the samples in an N-sample sliding window, proposed as:

$$X = \begin{bmatrix} Y(1) & Y(2) & \dots & Y(P+1) \\ Y(2) & Y(3) & \dots & Y(P+2) \\ \vdots & \vdots & \vdots & \vdots \\ Y(N-P) & Y(N-P+1) & \dots & Y(N) \end{bmatrix} \tag{4}$$

where N denotes the number of samples in the window, $Y(.)$ indicates the samples, P is the pencil parameter selected between N/3 to N/2 for filtering the noise [29]. The dimension of X is $(N-P)\times(P+1)$. A singular-value decomposition (SVD) is applied to the matrix X as follows:

$$Z = XX^H, \quad V = X^H X \tag{5}$$

$$X = U_Z \sum U_V^H \tag{6}$$

where $(.)^H$ and $U_{(.)}$ denote complex conjugate and a unitary matrix comprising eigenvectors, respectively. $\sum$ shows a diagonal matrix with the singular values of X, and the η_d is considered to select the dominant singular values as follows:

$$\eta_{max}\; 10^{-\kappa} \;\leq \eta_d \tag{7}$$

where κ is the filtering factor, η_d and η_{max} show the dominant and maximum singular value, respectively [29]. The columns of $\sum$ indicating the dominant singular values are stored and the remaining columns are omitted. As a result, the reduced matrix is named $\sum'$ [32]. Moreover, U_V is reduced to U'_V by keeping its columns associated with the dominant singular values and omitting the the rest of the columns [29]. Then, new matrices X_{last} and X_{first} are obtained, defined as follows:

$$X_{last} = U_Z \sum' U'^H_{V,last} \;\;,\;\; X_{first} = U_Z \sum' U'^H_{V,first} \tag{8}$$

where $U_{V,last}$ is calculated by omitting the last row of U'_V and $U_{V,first}$ is driven by deleting the first row of U'_V. In the next step, the eigenvalues of $X^+_{last}X_{first}$ are obtained, and $(.)^+$ represents Moore–Penrose pseudoinverse. The relation

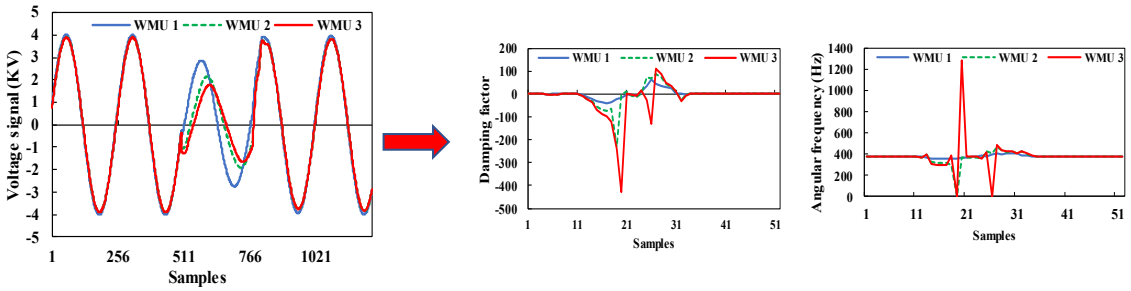

Fig. 2. Extracting modal features such as damping factor and angular frequency from the raw (sinusoidal) data

between the complex frequencies and eigenvalues is defined as follows [29]:

$$\lambda_i = e^{(-\alpha_i \pm j\omega_i)T_s}, \quad \forall i = 1, 2, \cdots, m \tag{9}$$

where T_s shows the sampling period and λ_i is the eigenvalues. In each snapshot, the complex frequencies are represented as (10) after the calculation of the eigenvalues [32].

$$\alpha_i(t) \mp j\omega_i(t) = -ln(\lambda_i)/T_s, \quad \forall i = 1, 2, \cdots, m \tag{10}$$

The steps described in (4)–(10) are repeated for each sensor in each snapshot.

C. Feature selection of WMU data

Modal analysis is conducted using STMPM on WMU data to characterize the dynamics of the distribution grids during the faults. A set of features consisting of modes with damping factors and angular frequencies and the corresponding residues for each of the modes is obtained. In order to distinguish the fault location, it is important to use the most informative features among all calculated features in each sliding window and the corresponding modes and residues. To this end, several steps are defined as follows to reduce the number of features into a manageable number for each sensor, defined as a new subset of the feature vector.

- Calculating the dominant modes and corresponding residues of the signal in each snapshot captured by the sliding window. This is done by forming matrix X and applying SVD on it as explained in Section II. In this study, the length of the window is assumed to be one cycle, and the step size of sliding over the signal is 10% of the window's length. Also, filtering factor κ is set on 3, and P is selected to be 83 as the pencil parameter based on the defined ranges.
- Selecting the mode that has the highest residue in each snapshot compared to the obtained modes. The damping factor and angular frequency of this selected mode are stored in the sub-set feature vector of each WMU.
- Continuing to store the modes' information until the sliding window passes the last sample of the signal, here is at the end of 5 cycles. At this point, a stream of data consisting of damping factor and angular frequency is obtained for each sensor with a shorter length and more informative information compared to the raw sinusoidal WMU data.

The illustrative example of mode decomposition using STMPM for raw signals captured from three WMU sensors is shown in Fig. 2. The asymmetrical ABG fault occurs where sensor 3 is located in the IEEE 13-bus system. As shown in this figure, the damping factor and angular frequency observed by WMU 3 have more significant variations compared to other sensors because fault causes more oscillations and creates new modes where it happens and in the adjacent area. For instance, the base fundamental angular frequency is roughly 377 $\approx 2\pi$ 60 Hz, but during the fault, it raises to more than 1200 Hz. It also reaches zero, showing the constant behavior of sinusoidal signal instantly after occurring fault in the limited points. The feature dimension associated with each sensor reduces to 104 = 52 features for damping factor and 52 features for angular frequency, which are less than 10% of the original feature dimension on raw data. The obtained features contain more informative and useful information for fault location as they contain the dynamic responses of the grid under the event.

III. Grid-informed data-driven Model

The topology of a distribution grid with installed WMUs is represented as a graph consisting of edge and nodal signals. The nodal information refers to the sensors' recorded data such as voltage and current, and the edge information is related to the physical characteristic of grid lines and their connectivity status. The grid-informed GNN enables us to process the feature nodes and grids into the graph convolution layers (GCNs). These layers are the substantial parts of the GNN structure. Two spatial and spectral convolution models are defined [33]. In a spatial model, driven by convolution networks, the information is aggregated from adjacent nodes of a particular node throughout the graph. Moreover, the input data must be in a single-dimension stream of data or two-dimension regular figures for convolution networks. Nevertheless, the conventional convolution network lacks a theoretical basis and cannot be implemented on a signal with spatial features [20]. However, the spectral-based convolution provides the chance to aggregate the spatial features more efficiently even on irregular shapes and graphs because of the strong theoretical basis in signal processing [20], [33]. The background and detailed explanations of the proposed grid-informed method are scrutinized in the following sections.

A. Theory of graphs

In this study, the distribution network is defined as an undirected graph $\mathbb{G} = (M, H, A)$, where M is the set of nodes, H shows the set of edges, and the adjacency matrix of $\mathbb{G}$ is given as A. A typical element of adjacency matrix A, showing the relationship between nodes n and m, is l_{nm}. The element has weighted and zero values if the connection exists and if it does not exist, respectively.

The adjacency matrix A describes the spatial relationship between the measurement devices in various locations. The weighted values are considered to indicate the correlation strength of the nodes and sensors recording system states. Nodes with stronger correlations, have larger l_{nm}. For instance, the closer nodes have a higher correlation and are affected somehow correspondingly under the occurrence of a fault in distribution grids. Thus, a distance-based metric is given as $l_{nm} = 1/d_{nm}$, where d_{nm} defines the geographical distance of two nodes [22]. The inverse relationship between the edge weights and the distance implies that closer distances of nodes correspond to higher correlation among them, which is a reasonable realization of fault analysis in power systems. Additionally, D is the diagonal degree matrix for the graph, showing the number of nodes connected to the corresponding node.

B. Graph convolution network

Multiplication of signal z, containing node voltages, with a parameterized filter b_θ is the spectral convolution in the Fourier domain. The convolution of the graph is defined as (11), where U contains the eigenvectors of the normalized Laplacian graph L as (12). The eigen decomposition performed on the normalized Laplacian graph L is shown in (13). In (13), $\Phi = diag\,(\lambda_1,\lambda_2,\lambda_3, \cdots ,\lambda_n)$ has ordered positive eigenvalues in a diagonal fashion.

$$b_\theta * z = U\, b_\theta\, U^T z \tag{11}$$

$$L = I - D^{-0.5}\, A\, D^{-0.5} \tag{12}$$

$$L = U \Phi U^T \tag{13}$$

The convolution operation on the graph, indicated in (11), has computational burden [20]. To alleviate this problem, b_θ which is a function of eigen values as $b_\theta(\Phi)$ can be defined approximately with the truncated Chebyshev polynomial expression with P^{th} order as (14) [34]. This simplification stabilizes the training process in filters [33]. Also, Chebyshev coefficients are represented in vector $\theta^{'}$, and the re-scaled representation of the eigenvalues is defined as (15). In (15), λ_{max} indicates the maximum eigenvalue of L.

$$b_{\theta'}(\Phi) \approx \sum_{p=0}^{P} \theta_p^{'} T_p(\hat{\Phi}) \tag{14}$$

$$\hat{\Phi} = 2/\lambda_{max} \times \Phi - I \tag{15}$$

The Chebyshev polynomials are defined recursively as $T_p(q) = 2yT_{p-1}(q) - T_{p-2}(q)$ [34]. The convolution of the filter and signal is simplified as (16), considering the $(U\Phi U^T)^p = U\ \Phi^p\ U^T$ property. In this equation, the scaled Laplacian matrix $\hat{L}$ is defined as (17).

$$b_{\theta'} * z \approx U \sum_{p=0}^{P} \theta_p^{'} T_p(\hat{\Phi})\, U^T z = \sum_{p=0}^{P} \theta_p^{'} T_p(\hat{L}) z \tag{16}$$

$$\hat{L} = 2/\lambda_{max} \times L - I \tag{17}$$

The order of (16) is P^{th}, meaning that it is P-localized and depends on maximum P adjacent nodes of the particular node [33]. In the next section, it is discussed about the optimal order of Chebyshev terms.

C. Reformulation of graph convolutions

The equation given in (16) is approximated by setting P equal to 1, considering the first two terms of the formulation [20]. Since the first terms of the truncated Chebyshev polynomials are as $T_0(q) = 1$ and $T_1(q) = q$, the obtained equation is a linear function of matrix L. It is discussed in [20] that this approximation helps us to design a deeper structure having less complexity compared to conventional models [33], and reduces the over-fitting. Moreover, the convolution on the graph is further simplified with $\lambda_{max} = 2$, so the reformulation of (16) is represented as follows:

$$b_\theta * z \approx \theta\,(I + D^{-0.5} A D^{-0.5})\, z \tag{18}$$

The coefficients of Chebyshev formulation are approximated with a single parameter $\theta = \hat{\theta}_0 = - \hat{\theta}_1$, representing the first and second terms. The eigenvalues' range in $I+D^{-0.5}AD^{-0.5}$ is defined as [0, 2], which causes vanishing gradients. A renormalization method is adopted to compensate the drawback of equation (18) [20]. The final representation of GNN convolution is proposed in (19), where $\hat{A} = I + A$, and $\hat{D}_{ii} = \sum_j \hat{A}_{ij}$ are used.

$$b_\theta * z \approx \theta\,(\hat{D}^{-0.5} \hat{A}\, \hat{D}^{-0.5})\, z \tag{19}$$

Equation (19) is then generalized by considering matrix $Z \in R^{N \times M}$ instead of z vector as (20). The stream of data has M features recorded by WMUs (before and after occurring fault). The matrix $\Omega \in R^{M \times Q}$ represents the parameter of filters with Q feature maps, and graph convoluted signals are given in matrix G.

$$G = (\hat{D}^{-0.5} \hat{A}\, \hat{D}^{-0.5})\, Z\, \Omega \tag{20}$$

D. Proposed GNN framework

The GNN structure with two GCN layers is given in (21). $W^{(0)} \in R^{M \times P}$ is the input of weight matrix with P feature maps, as shown in (21). Furthermore, $W^{(1)} \in R^{P \times Q}$ represents the weight matrix in the GCN layer.

GCN layers can store the average weighted data of sensors located on different nodes of the graph. The GCN outputs are passed by the last linear layer preceding the classifier, and the obtained values are given to the softmax, known as the multi-class classifier, represented as (22). Here, V is the weight matrix in the linear layer, which gives F to the softmax classifier. The classifier specifies the label vector Y which is the fault location using (22). Additionally, the cross-entropy

loss function is selected in this model [20]. The parameters are optimized in the GNN model using the iterative-based back-propagation algorithm. The loss function is optimized using the updated parameters with respect to the predicted Y and actual labels.

$$G = \hat{A}ReLU(\hat{A}ZW^{(0)})W^{(1)} \tag{21}$$

$$Y = softmax(F(G, V)) \tag{22}$$

E. Fault Location Problem

The STMPM and GNN are deployed for the two-stage feature engineering and fault location problem, as shown in Fig. 3. The feature selection stage is adopted to extract the modal data of raw signal recorded by sensors in various locations before, during, and after the occurrence of fault. The modal information represents the dynamic response of the grid against the fault. The selected informative data, which are damping factors and angular frequencies combined with the topological characteristics of the grids are considered as the input of the GNN, set in the second stage. Note that the weighted adjacency matrix includes the grid features such as lines' connectivity status, distance-based feature of lines, and the correlation strength of nodes including sensors. The selected modal features, containing the dynamic response of the grid, are ordered in matrix $Z \in R^{N\times M}$, where N shows the number of nodes in the network and M is the length of the selected features from WMUs. k nodes out of all N nodes are equipped with WMUs, indicating the scarce data availability in this analysis due to the high costs of these sensors. The feature vector of each sensor contains an informative short stream of damping factors and angular frequencies obtained by STMPM on the sinusoidal voltage signal.

The engineered features of raw data are given to the GCN layers. The rectified linear activation unit (ReLU) is set between GCNs. The mean pooling is performed after by the GCN layer to improve the localization accuracy. Additionally, a dropout layer is set for preventing overfitting. The output of the GCN layer is sent to the final linear layer preceding the softmax classifier. The Pytorch Geometric library is used to prepare the GNN framework [35].

IV. Case Study and Simulation Setup

The proposed model is evaluated on the modified IEEE 13-bus network to locate the faults, as shown in Fig. 4. The test system's nodes are labeled for this problem, and a non-dispatchable DER with a total capacity of 1 MW is added to bus 6. The synchronous generator is used as the DER in this simulation performed in PSCAD software [36], and is adjusted to operate as a non-dispatchable generation unit.

Also, three WMUs with a sampling rate of 256 per cycle are assumed to be installed at nodes 1, 6, and 8. The waveform signals observed in three nodes are recorded from the PSCAD simulation automated by Python interface considering various loads, DER generation, fault type, fault location, and fault impedance scenarios to prepare a realistic data-set under different operational conditions. To be more specific, the conditions are created by different DER power generation varying between 10% to 130% of the base capacity and loads changing from 80% to 130% of the base load to consider their stochastic behavior during different time slots [37]. Also, several symmetric and asymmetric faults are simulated in six locations. The impedance of faults is 0.01, 1, and 10 ohm. It needs to be noted that 6 different labels corresponding to different fault locations are considered, as shown in Fig. 4 with red-colored nodes and we are trying to find the location of these faults using STMPM and GNN. However, we have access to the raw and high sampling rate data of just three nodes due to the scarcity of WMU measurements. Therefore, the grid's topological feature and modal dynamic information of sensors are used in the proposed two-stage technique shown in Fig. 3 to tackle these challenges.

It is important to set up the model efficiently. In this regard, two GCN layers with 128 channels are set for GNN model [20], followed by a linear layer with 256 hidden nodes. The dropout rate is 0.5, and the learning rate of the Adam optimizer is selected to be 0.001. The batch size is adjusted at 8, and the maximum epoch number is 100 or 150. 70 % of data is used for training, 15% for validation, and 15% is considered for testing the model. The parameters of the STMPM are adjusted based on the approach discussed in II-C. All parameters are selected based on the search-based experiments and our previous studies [22] to get better results and reduce the computation time.

V. Results and Analysis

In this section, the proposed model is tested under different cases to locate the fault. A comprehensive comparison is also presented to show the competence of proposed methods.

A. Base case

In this section, 4320 scenarios are simulated for fault location considering the aforementioned conditions. Then, STMPM is adopted to extract the crucial features for fault localization. To evaluate the performance of the fault localization, the macro-average F1 (M-F1) score is also reported as (23). F1 score is defined through the harmonic mean of precision (PRE) and recall (REC) for each class $\Im$. The class set is shown with $\Re$. PRE indicates the classifier's ability for predicting true positives (TPs) in class $\Im$ among all TPs and predicted false positives (FPs) in the related label. The macro average of PRE (M-PRE) is defined as (24). Moreover, REC shows the classifier's performance in predicting TPs in class $\Im$ between all TPs and false negatives (FNs) corresponding to the $\Im$. In (25), the macro average of REC (M-REC) is defined for multiple classes. The accuracy and M-F1 score for this case study are 100% and 100%, respectively. Note that different transient symmetrical and asymmetrical faults with 1 cycle duration, known as challenging events, happen in the active network and the proposed method locates them precisely. All scores are calculated using the average of four independent training processes for this case and the following case studies.

$$M - F_1 = \sum_{\Im=1}^{\Re} \frac{2\ PRE_{\Im} * REC_{\Im}}{\Re * (PRE_{\Im} + REC_{\Im})} \tag{23}$$

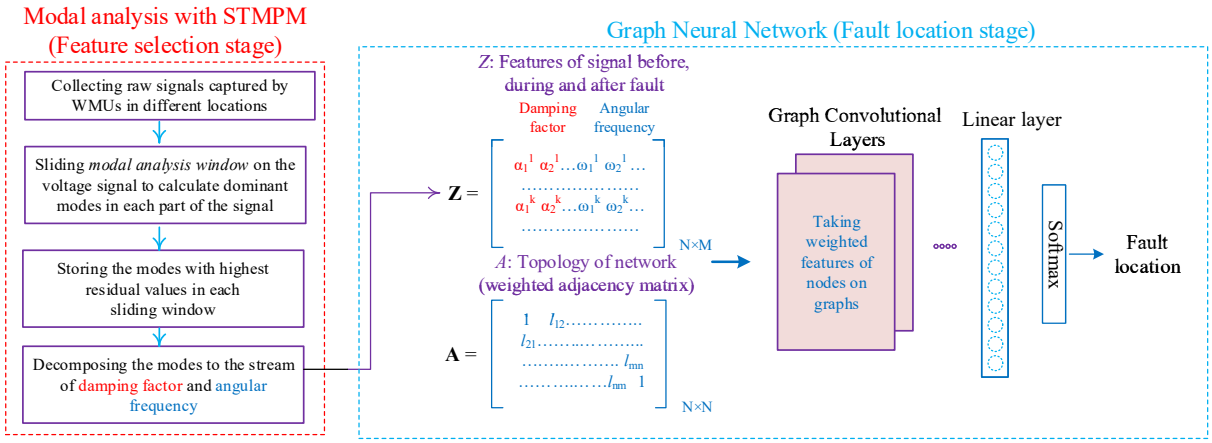

Fig. 3. The structure of proposed method for identifying fault location

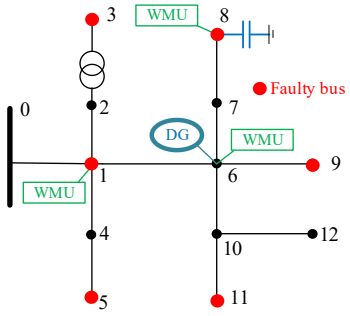

Fig. 4. Schematic of the modified IEEE 13-bus network

$$M-PRE=\frac{\sum_{\Im=1}^{\Re} TP_{\Im}/(TP_{\Im}+FP_{\Im})}{\Re} \tag{24}$$

$$M-REC=\frac{\sum_{\Im=1}^{\Re} TP_{\Im}/(TP_{\Im}+FN_{\Im})}{\Re} \tag{25}$$

B. Noisy data

The streamed waveform data of sensors may be affected by noises, reducing the quality of the signals and making the fault location analysis more challenging. To evaluate the robustness of the proposed method against the noisy data, this section addresses the localization problem considering different levels of signal-to-noise ratios (SNR). The extracted features with different fault impedance as 0.01, 1, and 10 ohms are stored for testing the method. As shown in Table III, by reducing the SNR to 15 as the worst scenario, the accuracy and M-F1 score decrease to 77.58% and 78.46%, respectively. This is due to the fact that the data are very noisy and noise variations are sometimes very similar to the voltage drop under the faults. However, the localization accuracy and M-F1 score attain 98.88% and 99.06 % with higher SNR as 45 dB [8]. All results are the average values under four experiments in 100 epochs using 4320 samples.

TABLE I
THE IMPACT OF THE NOISE ON THE MODEL'S PERFORMANCE

SNR (dB)	45	35	25	15
ACC %	98.88	95.13	87.57	77.58
M-F1 %	99.06	95.90	88.84	78.46

C. Sampling rates

The WMU sensors may have different sampling rates, depending on their technology. Higher sampling rate sensors obtain more information in a short period of time like 1 cycle, but more communication and storage resources are required for transmitting and storing this large data set. The impact of the sampling rate of sensors is evaluated in the section, by down-sampling the data to 50% and 33% of the original signal samples. In STMPM algorithm, the length of the window and sliding steps are kept as discussed before. Therefore, the extracted data length is reduced to 52 and 34 in 50% and 33% down-sampling, respectively. According to the result shown in Table II, the average accuracy and M-F1 scores are still at desirable levels although a significant part of the information is missing. The original data set with SNR 45 used in sub-section V-B is adopted for this section.

TABLE II
THE SUB-SAMPLING IMPACT ON THE MODEL'S PERFORMANCE

Sub-sampling %	50	33
ACC %	97.68	96.29
M-F1 %	98.08	96.92

D. Configuration of sensors

Synchronous waveform measurements are still not very common in distribution networks, and usually, a few WMUs are located to collect spatial-temporal information for event analysis. Here, we analyze the performance of the proposed model for as few as two sensors in three possible configurations. Three configurations of two sensors are specified as A: [1, 6], B: [1, 8], and C: [6, 8]. The location of WMUs are chosen heuristically on three-phase nodes to enhance the observable area of the network. Optimizing the location and

number of sensors is not within the scope of this paper. The fault location accuracy is over 99% for configuration B and C. However, the accuracy and M-F1 scores reduce to 95.37% and 96.14%, respectively, when two WMUs are located on nodes 1 and 6, indicating set A. Still, we can claim that the performance of the model is robust against different configurations with a minimum number of sensors to capture the spatial-temporal correlation of nodes over the grid. The data set of sub-section V-B with SNR 45 is considered for this assessment.

TABLE III
THE IMPACT OF WMU CONFIGURATION ON LOCALIZATION

WMUs configuration	A	B	C
ACC %	95.37	99.03	99.92
M-F1 %	96.14	99.22	99.93

E. Fault duration

Suppose a permanent fault occurs and lasts until the end of the WMU's recording period. This fault may be cleared with protection devices as it doesn't have self-cleaning capability. Intentionally, fewer samples (3360 samples) with random inception angles, are generated under different load and DER power generation, as in real-world situations, we may not have access to enough historical event data and events can occur at any inception angle. The inception angles are equally divided into four points before and four points after the previously fixed angle on a particular cycle. The fault impedances are 0.01 and 1 ohm, and both symmetrical and asymmetrical faults are considered under different noise levels of 35 dB and 45 dB. The fault location average accuracy and M-F1 scores are 95.53% and 96.04%, respectively. These are the average scores under four independent experiments (training and testing) with the same data set. Identifying this fault enhances electrics' safety and situational awareness because these permanent/multi-cycle faults lie within the severe faults, increasing the risk of apparatus failures and life-threatening matters.

F. Comparison with state-of-art models

The performance of the proposed model is compared with other methods such as Decision tree (DT), Logistic regression (LR), and k-nearest neighbors (kNN). Sklearn package is used for the implementation of these baseline models. The kNN algorithm classifies an unknown sample using the predefined labels of its closest neighbors [38]. DT method constructs the branches as conjunctions of features and leaves as class labels. Both kNN and DT are evaluated extensively in [39], showing their acceptable performance in the event classification of distribution grids. LR is an efficient and simple algorithm, used for multi-class classification [40]. When less labeled data are available, a less complicated algorithm like LR can lead to higher accuracy than complex methods, as discussed in [41].

Tuning parameters: To conduct a fair comparison, the parameters are tuned with the same data set in four independent experiments. DT is tuned by evaluating the depth of the tree and testing several values such as $3, 10, 20, 50$, and 100. As

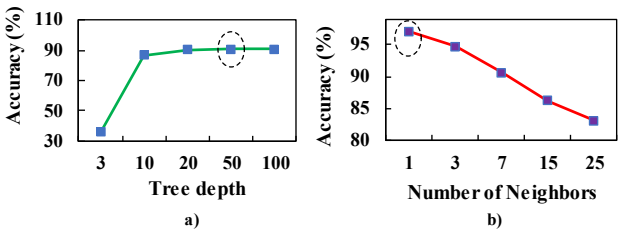

Fig. 5. Process of hyperparameter tuning

for kNN, k parameter, showing the number of neighbors, is selected from $1, 3, 7, 15$, and 25 candidate values in a search-based manner. These parameters have a considerable impact on the performance of the baseline models, as shown in Fig. 5. The optimal parameters are 50 and 1 for DT and kNN models, respectively, and are indicated with dotted circles in Fig. 5. The average accuracy of four experiments is the criteria, as shown on the y-axis of Fig. 5, to find the optimal values for these parameters. As LR has a simple structure, a large maximum iteration is set to 3000 for the convergence, improving the classification accuracy with $lbfgs$ optimizer and $L2$ penalty [22].

Table IV shows comparisons between the graph-based approach and baseline models. The proposed feature engineering technique, STMPM, is combined with all ML methods. Two other metrics such as M-PRE and M-REC scores, introduced in V-A, are considered to show more details in the comparison. The transient fault data set in section V-B is completed with a new data set considering 8 new inception angles on a cycle. The angles are randomly selected during the process of data generation. Additionally, the data used in V-E, representing permanent fault events, are considered in this section. The study in this section is also conducted under significant noisy environments with 35 and 45 dB. Finally, 8880 samples are prepared for this section, addressing fault location and fault type event problems. Fault type refers to whether the fault is transient or permanent. Detecting the fault type increases situational awareness as the operator takes proper actions according to the possible consequences of the faults on the operation of grid apparatus and human safety. It is shown in Table IV that the accuracy and other statistical metrics for the proposed grid-informed model are better within 150 epochs compared to the baseline methods. The demonstrated scores are calculated by taking the average scores obtained in four individual experiments. Here, 70% of data is used for training, and 30% is selected for testing the models. As for baseline models, kNN performs very well and is comparable with GNN thanks to the extracted features by STMPM. Also, the performance of LR and DT is acceptable for the classification in overall.

To show the performance of the model for each class, a confusion matrix is presented in Fig. 6 for one of the experiments. The y-axis and x-axis show the actual and predicted classes, respectively. The off-diagonal elements show the error in locating the fault of the corresponding class in that particular row of the matrix. The labels are 0, 1, 2, 3, 4, and 5 for

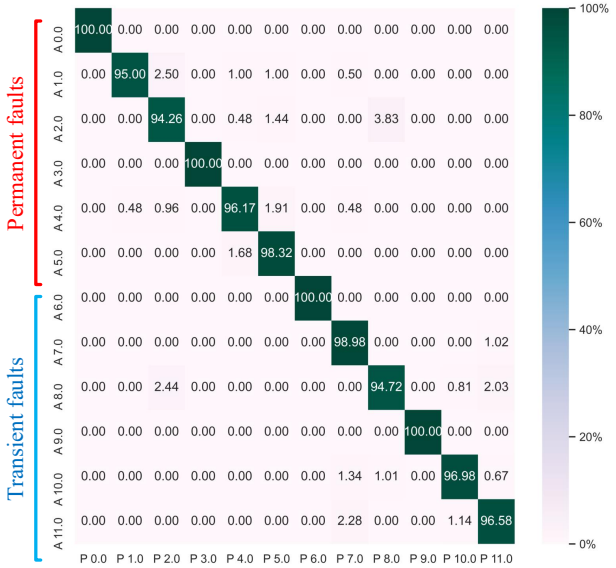

Fig. 6. Confusion matrix of GNN (A: Actual class, P: Predicted class

permanent faults, indicating faults occurring in nodes 11, 1, 3, 5, 8, and 9 on modified IEEE 13-bus, respectively. Also, labels 6, 7, 8, 9, 10, and 11 are related to the same locations considered in the permanent event but for transient faults. For instance, the proposed model misclassifies 2.44% of transient faults in location 3 (class 8) as permanent faults in the same location (class 2). However, the location of the fault is detected with acceptable accuracy, but the type of the fault is not well recognized for all scenarios of this class.

TABLE IV
THE COMPARISON OF RESULTS

Approach	ACC %	M-PRE %	M-REC %	M-F1 %
GNN	**97.15**	**97.33**	**97.34**	**97.31**
kNN	97.10	97.26	97.27	97.20
DT	90.85	91.15	90.89	90.99
LR	92.54	92.61	92.55	92.55

VI. Discussion and Future Directions

The proposed two-stage framework is a viable solution to locate faults and determine their type in distribution networks. Several merits of this study are discussed and future works are highlighted as follows:

Limited number of sensors: Although there are a few installed WMU sensors in grids due to their high costs, the proposed model captures their spatial-temporal correlation using the dynamic modes of the waveforms recorded by WMUs to locate the transient and permanent faults with good accuracy. Also, a different configuration of sensors is studied, and the robustness of the model in localization is proved again for as few as two sensors.

Data resolution: The emerging WMU sensors provide sinusoidal lengthy raw information with a high resolution. In this study, we assume that dominant features are selected using STMPM from these sinusoidal signals, enabling us to process fewer dimension data (10% of the original signal) with useful modal information for fault location and type classifications. The STMPM, an efficient feature selection technique, reduces computation time and enhances localization accuracy. In future studies, the shape-based feature extraction will be used on modal features [8], as a second layer of feature engineering, to reduce the feature dimension while improving the accuracy.

Data-based versus physics-based models: The proposed model is bridging both data-based and circuit-based fault locating problems using the GNN and STMPM. As shown in Table IV, data-based conventional models do not perform better in locating fault and identifying the fault type compared to the grid-informed GNN. On the other hand, pure circuit-based analysis requires accurate modeling of mutual impedance, various types of DERs and loads, unbalanced characteristics of lines, and hybrid networks with different overhead lines and/or cables. The feature of the network is included in our model with a weighted adjacency matrix. The components of this matrix show: 1) the connectivity status of nodes which is the grid topology, 2) the distance among the nodes related to the impedance of lines, and 3) the correlation of sensors indicating the highly affected nodes under the event for the particular node. Moreover, the STMPM also extracts the feature of the measured signals by sensors, reflecting the dynamic response of the grid under the events. Thus, the impact of the grid's physics is inherently included in the modal analysis as well.

As for future works, this study can be further improved considering more characteristics of faults such as arc modeling and higher impedance faults [42]. The data set will be also prepared using Real Time Digital Simulator (RTDS).

VII. Conclusion

This paper has proposed a two-stage fault location and type classification framework. In the first stage, the modal analysis was performed with the Short-Time Matrix Pencil method (STMPM) to capture the dynamic response of the grid during the transient and permanent faults using the recorded sinusoidal voltages by Waveform Measurement Units (WMUs), known as emerging class of sensors. The dominant modes consisting of damping factor and angular frequency were selected using STMPM as the engineered informative features. The selected features were given to the GNN model in the second stage to locate the faults and identify the fault type. The physical features of the distribution power grid and the locationally-scarce WMUs were considered during the training process using the weighted adjacency matrix and GCN filters that could capture spatial-temporal features over the grid. The efficacy and robustness of the model were verified using the modified IEEE test system considering a variation of DER and loads, noisy data, a different configuration of WMUs, the various sampling rates of WMUs, and different fault types. Statistical analysis showed that the proposed model classified better compared to other baseline models, such as KNN, DT, and LR. However, still simple algorithms like kNN can classify very good thanks to the implementation of the efficient feature extraction method, STMPM.

REFERENCES

[1] S. Wang and P. Dehghanian, "On the use of artificial intelligence for high impedance fault detection and electrical safety," *IEEE Transactions on Industry Applications*, vol. 56, no. 6, pp. 7208–7216, 2020.

[2] M. Izadi and H. Mohsenian-Rad, "Synchronous waveform measurements to locate transient events and incipient faults in power distribution networks," *IEEE Transactions on Smart Grid*, vol. 12, no. 5, pp. 4295–4307, 2021.

[3] A. F. Bastos, S. Santoso, W. Freitas, and W. Xu, "Synchrowaveform measurement units and applications," in *2019 IEEE Power & Energy Society General Meeting (PESGM)*. IEEE, 2019, pp. 1–5.

[4] S. Kulkarni, D. Lee, A. J. Allen, S. Santoso, and T. A. Short, "Waveform characterization of animal contact, tree contact, and lightning induced faults," in *IEEE PEs General meeting*. IEEE, 2010, pp. 1–7.

[5] T. S. Sidhu and Z. Xu, "Detection of incipient faults in distribution underground cables," *IEEE Transactions on Power Delivery*, vol. 25, no. 3, pp. 1363–1371, 2010.

[6] I. Niazazari, H. Livani, A. Ghasemkhani, Y. Liu, and L. Yang, "Event cause analysis in distribution networks using synchro waveform measurements," in *2020 52nd North American Power Symposium (NAPS)*. IEEE, 2021, pp. 1–5.

[7] W. Xu, Z. Huang, X. Xie, and C. Li, "Synchronized waveforms x2013; a frontier of data-based power system and apparatus monitoring, protection, and control," *IEEE Transactions on Power Delivery*, vol. 37, no. 1, pp. 3–17, 2022.

[8] Y. Liu, L. Yang, A. Ghasemkhani, H. Livani, V. A. Centeno, P.-Y. Chen, and J. Zhang, "Robust event classification using imperfect real-world PMU data," *IEEE Internet of Things Journal*, 2022.

[9] Y. Yuan, Z. Wang, and Y. Wang, "Learning latent interactions for event identification via graph neural networks and PMU data," *IEEE Transactions on Power Systems*, 2022.

[10] A. L. Liao, E. M. Stewart, and E. C. Kara, "Micro-synchrophasor data for diagnosis of transmission and distribution level events," in *2016 IEEE/PES Transmission and Distribution Conference and Exposition (T&D)*. IEEE, 2016, pp. 1–5.

[11] I. Niazazari and H. Livani, "A PMU-data-driven disruptive event classification in distribution systems," *Electric Power Systems Research*, vol. 157, pp. 251–260, 2018.

[12] M. Izadi and H. Mohsenian-Rad, "A synchronized lissajous-based method to detect and classify events in synchro-waveform measurements in power distribution networks," *IEEE Transactions on Smart Grid*, vol. 13, no. 3, pp. 2170–2184, 2022.

[13] M. MansourLakouraj, R. Hossain, H. Livani, and M. Ben-Idris, "Application of graph neural network for fault location in PV penetrated distribution grids," in *2021 North American Power Symposium (NAPS)*. IEEE, 2021, pp. 01–06.

[14] F. C. Trindade, W. Freitas, and J. C. Vieira, "Fault location in distribution systems based on smart feeder meters," *IEEE transactions on Power Delivery*, vol. 29, no. 1, pp. 251–260, 2013.

[15] S. Shi, A. Lei, X. He, S. Mirsaeidi, and X. Dong, "Travelling waves-based fault location scheme for feeders in power distribution network," *The Journal of Engineering*, vol. 2018, no. 15, pp. 1326–1329, 2018.

[16] M. Zhao and M. Barati, "A real-time fault localization in power distribution grid for wildfire detection through deep convolutional neural networks," *IEEE Transactions on Industry Applications*, vol. 57, no. 4, pp. 4316–4326, 2021.

[17] S. Xiong, Y. Liu, J. Fang, J. Dai, L. Luo, and X. Jiang, "Incipient fault identification in power distribution systems via human-level concept learning," *IEEE Transactions on Smart Grid*, vol. 11, no. 6, pp. 5239–5248, 2020.

[18] H. Liu, S. Liu, J. Zhao, T. Bi, and X. Yu, "Dual-channel convolutional network-based fault cause identification for active distribution system using realistic waveform measurements," *IEEE Trans Smart Grid*, 2022.

[19] W. Li, E. Xiang, and K. Wang, "Incipient fault identification in power distribution systems based on siamese temporal graph," in *2021 Power System and Green Energy Conference (PSGEC)*. IEEE, 2021, pp. 789–794.

[20] T. N. Kipf and M. Welling, "Semi-supervised classification with graph convolutional networks," *arXiv preprint arXiv:1609.02907*, 2016.

[21] K. Chen, J. Hu, Y. Zhang, Z. Yu, and J. He, "Fault location in power distribution systems via deep graph convolutional networks," *IEEE Journal on Selected Areas in Communications*, vol. 38, no. 1, pp. 119–131, 2019.

[22] M. MansourLakouraj, M. Gautam, H. Livani, and M. Benidris, "A multi-rate sampling PMU-based event classification in active distribution grids with spectral graph neural network," *Electric Power Systems Research*, vol. 211, p. 108145, 2022.

[23] M. MansourLakouraj, M. Gautam, R. Hossain, H. Livani, M. Benidris, and S. Commuri, "Event classification in active distribution grids using physics-informed graph neural network and pmu measurements," in *2022 IEEE Industry Applications Society Annual Meeting (IAS)*, 2022, pp. 1–6.

[24] A. Aligholian and H. Mohsenian-Rad, "GraphPMU: Event clustering via graph representation learning using locationally-scarce distribution-level fundamental and harmonic pmu measurements," *arXiv preprint arXiv:2205.13116*, 2022.

[25] R. Rezaiesarlak and M. Manteghi, "Accurate extraction of early-/late-time responses using short-time matrix pencil method for transient analysis of scatterers," *IEEE Transactions on Antennas and Propagation*, vol. 63, no. 11, pp. 4995–5002, 2015.

[26] A. Bagheri, I. Y. Gu, M. H. Bollen, and E. Balouji, "A robust transform-domain deep convolutional network for voltage dip classification," *IEEE Transactions on Power Delivery*, vol. 33, no. 6, pp. 2794–2802, 2018.

[27] O. Gashteroodkhani, M. Majidi, and M. Etezadi-Amoli, "A combined deep belief network and time-time transform based intelligent protection scheme for microgrids," *Electric Power Systems Research*, vol. 182, p. 106239, 2020.

[28] J. F. Hauer, C. Demeure, and L. Scharf, "Initial results in prony analysis of power system response signals," *IEEE Transactions on power systems*, vol. 5, no. 1, pp. 80–89, 1990.

[29] T. Sarkar and O. Pereira, "Using the matrix pencil method to estimate the parameters of a sum of complex exponentials," *IEEE Antennas and Propagation Magazine*, vol. 37, no. 1, pp. 48–55, 1995.

[30] L. L. Grant and M. L. Crow, "Comparison of matrix pencil and prony methods for power system modal analysis of noisy signals," in *2011 North American power symposium*. IEEE, 2011, pp. 1–7.

[31] R. Rezaiesarlak and M. Manteghi, "Short-time matrix pencil method for chipless rfid detection applications," *IEEE Transactions on Antennas and Propagation*, vol. 61, no. 5, pp. 2801–2806, 2013.

[32] R. J. Hamidi, H. Livani, and R. Rezaiesarlak, "Traveling-wave detection technique using short-time matrix pencil method," *IEEE Transactions on Power Delivery*, vol. 32, no. 6, pp. 2565–2574, 2017.

[33] M. Defferrard, X. Bresson, and P. Vandergheynst, "Convolutional neural networks on graphs with fast localized spectral filtering," *Advances in neural information processing systems*, vol. 29, pp. 3844–3852, 2016.

[34] D. K. Hammond, P. Vandergheynst, and R. Gribonval, "Wavelets on graphs via spectral graph theory," *Applied and Computational Harmonic Analysis*, vol. 30, no. 2, pp. 129–150, 2011.

[35] "PyTorch Geometric." [Online]. Available: https://pytorch-geometric.readthedocs.io/en/latest/

[36] "Ver. 5 PSCAD/EMTDC (software package), University of Manitoba, Winnipeg, MB, Canada."

[37] M. Mansour-lakouraj and M. Shahabi, "Comprehensive analysis of risk-based energy management for dependent micro-grid under normal and emergency operations," *Energy*, vol. 171, pp. 928–943, 2019.

[38] N. García-Pedrajas, J. A. R. Del Castillo, and G. Cerruela-Garcia, "A proposal for local k values for k-nearest neighbor rule," *IEEE transactions on neural networks and learning systems*, vol. 28, no. 2, pp. 470–475, 2015.

[39] A. Shahsavari, M. Farajollahi, E. M. Stewart, E. Cortez, and H. Mohsenian-Rad, "Situational awareness in distribution grid using micro-PMU data: A machine learning approach," *IEEE Transactions on Smart Grid*, vol. 10, no. 6, pp. 6167–6177, 2019.

[40] M. Coutinho, L. L. Novo, M. de Melo, L. de Medeiros, D. Barbosa, M. Alves, V. Tarragô, R. dos Santos, H. L. Neto, and P. Gama, "Machine learning-based system for fault detection on anchor rods of cable-stayed power transmission towers," *Electric Power Systems Research*, vol. 194, p. 107106, 2021.

[41] N. T. Bazargani, G. Dasarathy, L. Sankar, and O. Kosut, "A machine learning framework for event identification via modal analysis of PMU data," *arXiv preprint arXiv:2202.06836*, 2022.

[42] M. Afshar, M. Majidi, O. A. Gashteroodkhani, and M. E. Amoli, "Analyzing performance of relays for high impedance fault (HIF) detection using hardware-in-the-loop (HIL) platform," *Electric Power Systems Research*, vol. 209, p. 108027, 2022.